Comparison of Hydrogen Bonding in 1-Octanol and 2-Octanol as Probed by Spectroscopic Techniques

Francesca Palombo,[†] Paola Sassi,[†] Marco Paolantoni,*[,†] Assunta Morresi,[†] and Rosario Sergio Cataliotti[‡]

Dipartimento di Chimica, Università di Perugia, Via Elce di Sotto, 8, I-06100 Perugia, Italy, and Istituto Nazionale di Fisica della Materia, Unità di Catania, V.le A. Doria, 6, I-95125 Catania, Italy

Received: April 28, 2006; In Final Form: July 19, 2006

Liquid 1-octanol and 2-octanol have been investigated by infrared (IR), Raman, and Brillouin experiments in the 10−90 °C temperature range. Self-association properties of the neat liquids are described in terms of a three-state model in which OH oscillators differently implicated in the formation of H-bonds are considered. The results are in quantitative agreement with recent computational studies for 1-octanol. The H-bond probability is obtained by Raman data, and a stochastic model of H-bonded chains gives a consistent picture of the self-association characteristics. Average values of hydrogen bond enthalpy and entropy are evaluated. The H-bond formation enthalpy is ca. −22 kJ/mol and is slightly dependent on the structural isomerism. The different degree of self-association for the two octanols is attributed to entropic factors. The more shielded 2-isomer forms larger fractions of smaller, less cooperative, and more ordered clusters, likely corresponding to cyclic structures. Signatures of a different cluster organization are also evidenced by comparing the H-bond energy dispersion (HBED) of OH stretching IR bands. A limiting cooperative H-bond enthalpy value of 27 kJ/mol is found. It is also proposed that the different H-bonding capabilities may modulate the extent of interaggregate hydrocarbon interactions, which is important in explaining the differences in molar volume, compressibility, and vaporization enthalpy for the two isomers.

Introduction

Hydrogen bond (HB) interactions regulate the structure, reactivity, and dynamics of basic components in all living organisms, and they also control the association of many molecules. Aliphatic alcohols are amphiphilic self-associating molecules constituted of a polar hydroxyl head and an alkyl tail, which form complex hydrogen bond networks. Even as neat liquids, alcohols are heterogeneous on microscopic scales, and the existence of hydrophobic and hydrophilic environments in dynamical equilibrium must be considered.

The strength of the hydrogen bond interactions, the degree of self-association, and the geometrical arrangements of local environments in the liquid state are in some way correlated with the length and branching of the hydrocarbon tail and with the different exposure of the OH group.[1−7] The same molecular factors also regulate relaxation processes and dynamical properties of the liquid systems.[8−11] In amphiphilic molecules, two types of forces take part in determining overall liquid organization, namely, the dispersion forces concentrated on the hydrocarbon tails (i.e., "hydrophobic") and the dipolar electrostatic ones localized on the OH groups (i.e., "hydrophilic"). These forces are correlated, and their interplay, determining the structure and the dynamics of the liquid at molecular scales, modulates its macroscopic properties.

It is generally accepted that secondary and tertiary alcohols are less associated than the linear ones, and the shielding on the polar head is thought to increase the fraction of cyclic species over linear aggregates dominating in *n*-alcohols.[1,3,5−7] Apart from the large number of studies on the self-association properties of alcohols, an in-depth investigation involving a comparison of different spectroscopic data is still missing, and quantitative information on the different properties in isomers with relatively long-chain portions is scarcely available. Recently, several computational and experimental studies were performed on the shortest members.[3,11−13] Monte Carlo simulations indicate that overall liquid structure and the aggregate distribution of 1- and 2-propanol are very similar, while significant differences are detected for *tert*-butyl alcohol.[3] Other authors found evidence that the strength and the stability of H-bonds is enhanced in 2-propanol.[11−13] In fact, in the solid and glassy states 2-propanol presents a higher order at short distances and a lower order at intermediate length scales than 1-propanol. This explains both the higher melting and glass transition temperatures of 2-propanol as well as its lower density. This picture expresses the complex role played by the counterbalance between electrostatic and van der Waals interactions in two relatively small systems in which the structural isomerism mainly affects the molecular shape.[11−13]

In the present study, a detailed investigation of the energetic and structural properties of 1-octanol (1-oct) and 2-octanol (2-oct) neat liquid systems is performed by means of different spectroscopic techniques (Raman, infrared, and Brillouin) and using various spectral analysis procedures. The aim is to provide a quantitative microscopic description of the changes induced by the differing OH positioning in two isomers in which large contributions derive from hydrocarbon interactions and where the molecular shape is not drastically perturbed. This may help explain on a molecular basis the difference in thermal and macroscopic properties. We note that the minor change in the

* Corresponding author. Phone: +39 075 585 5580. Fax: +39 075 585 5598. E-mail: marcopa@unipg.it.
[†] Università di Perugia.
[‡] Istituto Nazionale di Fisica della Materia.

10.1021/jp062614h CCC: $33.50
Published on Web 08/22/2006

TABLE 1: Comparison of Several Macroscopic and Microscopic Data of 1-Oct and 2-Oct

	1-oct	2-oct
T_{fus}/K	257	235
T_{boil}/K	468	453
T_c/K	653	632
ΔH_{vap}/kJ mol^{-1}	70.2[a]	67.5[a]
P_{vap}/Pa	10.9[b]	32.8[b]
η/cP	9.0 ± 0.1[c]	8.7 ± 0.1[c]
d/g cm^{-3}	0.8213[b]	0.8161[b]
V_m/cm^3 mol^{-1}	158.6[d]	159.6[d]
V_w/g cm^{-3}	92.68[d]	92.62[d]
V_{void}/g cm^{-3}	65.9[d]	67.0[d]
χ_s^{hy}/GPa^{-1}	0.58 ± 0.02[e]	0.66 ± 0.02[e]
χ_s^{ul}/GPa^{-1}	0.669 [f]	0.701 [f]

[a] At 298 K as derived from the group scheme of ref 64. [b] Interpolated from the data of ref 41 at 298 K. [c] This work at 293 K. [d] V_m is the molar volume, V_w is the intrinsic molar volume calculated with the increments of ref 42, and V_{void} is the free volume, $V_{void} = V_m - V_w$. [e] Isoentropic compressibility, from hypersonic velocities at 298 K. [f] Isoentropic compressibility from ultrasonic velocities from the data of ref 28 at 298 K.

molecular structure influences a number of basic thermodynamic properties (see Table 1).

The 1-oct liquid system is especially significant, constituting the typical nonpolar phase employed in standard partitioning studies.[14,15] The partition of a biorelevant solute in the water/octanol system is strictly correlated to its pharmacokinetic properties and biological activity. Consequently, liquid 1-oct has been subjected to numerous experimental and computational studies to elucidate its supramolecular organization.[5,16−26] Minor discrepancies aside, an overall consensus on its basic structural properties has been achieved mainly thanks to recent computational studies.[22−26] In this regard, experimental results derived from spectral analysis methods can be compared to timely simulation findings, and further applied on 2-oct, in which analogous studies have not been carried out. It is worth noting that lately, as a refinement of the 1-oct/water model system, the use of a pool of four solvents with different properties to account for the different biophysical properties of membranes has been considered.[27,28] Within this framework, 2-oct may be regarded as an alternative amphiphile to 1-oct.

The infrared (IR) and Raman OH stretching distributions are described considering the existence of different types of oscillators. In this respect, employing both techniques in parallel is expected to improve the results previously obtained considering the IR spectra of 1-oct.[21] The population of different species and the relative enthalpy and entropy of H-bond formation are obtained. A stochastic model, analogous to the percolation model of water, is also applied to describe the self-association characteristics of these liquids.[29−31] Moreover, the H-bond energy dispersion (HBED), recently employed to gain insights on the energetics of H-bonded liquids,[4,21,32−34] is tested as a probe of the structural changes in the two isomers. The quantitative analysis proposed extends our recent studies in which differences on the supramolecular organization of the two isomers have been related to the Raman noncoincidence effect (NCE)[4] that depends on the geometrical arrangement among coupled oscillators.[35,36]

Finally, hypersonic velocities are obtained via Brillouin scattering experiments,[37,38] and the hypersonic compressibilities are evaluated for the two pure samples at different temperatures. Since H-bonded networks show a marked tendency to preserve their configuration,[39] the compressibility of microheterogeneous amphiphilic systems may provide information on the interchain potentials of the less rigid hydrophobic regions.

Experimental Section

1-Octanol and 2-octanol (racemic mixture) were supplied by Fluka at a purity of 99.0 mol % and were then used without any further purification. Viscosities at the various temperatures were measured with apparatus and methods described elsewhere.[40] FT-IR spectra were measured using a Bruker IFS 113V FT-IR spectrometer, with a resolution of 2 cm^{-1}, a one-level zero-filling, and a trapezoidal apodization. Cells with CsI windows were used without spacers. The spectra were run at room temperature in the range of 400−4000 cm^{-1} and at different temperatures between 5 and 75 °C in the spectral region of the O−H stretching motion. Raman spectra were obtained using a U-1000 grating double monochromator (ISA Jobin-Yvon). The exciting source was an argon ion laser (Coherent, model Innova 90) operating at 514.5 nm with a power of 700 mW on the sample. The scattered intensity at 90° geometry was measured by a photon-counting unit using an electronically cooled Hamamatsu, model R943 photomultiplier detector. The spectra were recorded in the frequency range of 2600−3800 cm^{-1}, encoding intervals of 1 cm^{-1}, in the temperature range of 5−75 °C. The slit widths were adjusted to 250−500 μm for the external and intermediate slits, respectively. The spectral resolution was in this case 2.5 cm^{-1}. Brillouin spectra were acquired in the 90° geometry by using the monomode (Etalon intracavity) 514.5 nm radiation of a COHERENT Innova 90 argon ion laser; the sample was irradiated with 300 mW of power. By placing the free spectral range of our single-pass piezo-scanned Fabry−Perot interferometer (Burleigh RC-110) at the value of 20 GHz, with a finesse of 30 ca., we can record three orders of the interferometric trace by means of a Hamamatsu Photonics H7421-40 photomultiplier tube. The statistics of measurement were improved further with many (at least 10) acquisitions. In all experiments, the temperature was controlled by circulating water from an ultrathermostat Haake, model F6, with a precision of 0.5 °C.

Results and Discussion

Density, Viscosity, and Hypersonic Compressibility. The secondary alcohol has larger molar volume (V_m) at all of the temperatures considered,[41] by effect of a less extended and/or different H-bond structure. The two isomers have almost identical van der Waals volumes (V_w), as evaluated by an additive scheme[42] (92.68 and 92.62 cm^3 mol^{-1} for 1- and 2-oct, respectively). Thus the liquid 2-oct is characterized by a larger free volume (V_{void}). This latter measures the empty space between the molecules and depends on intermolecular interactions.[28]

Brillouin scattering spectra of the two alcohols were recorded between 5 and 70 °C, and the hypersonic velocities v_h were evaluated by the measured Brillouin shift.[37,38] The isoentropic compressibility χ_S was then calculated using the usual expression:

$$\chi_S = (v_h^2 \rho)^{-1} \quad (1)$$

where ρ is the mass density. In Figure 1, χ_S is reported for the 1- and 2-isomers at different temperatures. χ_S is considerably higher for 2-oct in the entire range investigated. It is expected that this quantity decreases going from linear alkanes to the corresponding alkanols due to increasing H-bonding forces and that the effect should be more important for shorter alcohols.[37,43] Thus, for the 2-isomer H-bonds are less effective in decreasing χ_S. The data also confirm that the χ_S is a very sensitive probe of intermolecular interactions, since important differences can

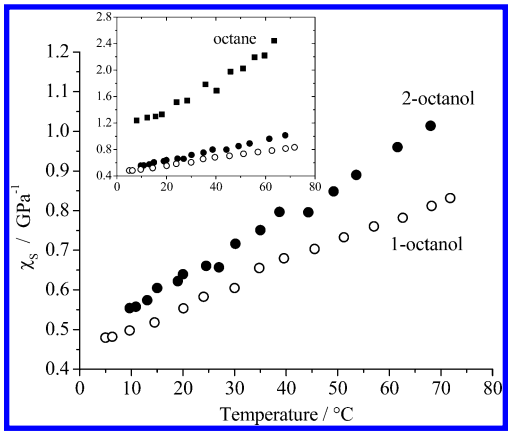

Figure 1. Isoentropic compressibility of 1-oct and 2-oct calculated form Brillouin data. A comparison with octane is reported in the inset.

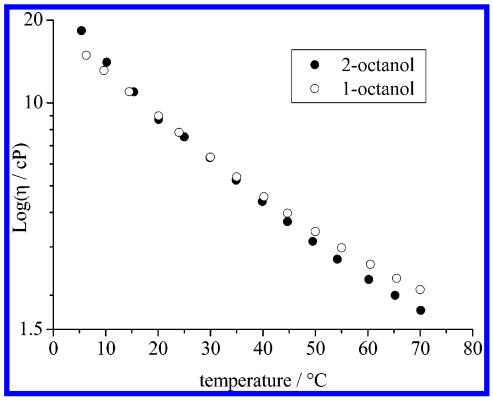

Figure 2. Viscosity of 1-oct and 2-oct at different temperatures.

be detected even for two systems with very similar densities and with not dramatic changes of the overall self-association degree (see below). The important role that may be played by hydrocarbon interactions on compressibility of alkanols is evidenced by the fact that its value decreases with increasing chain length. In this sense, the contribution *per* CH_2 group prevails over the reduced self-association.[43,44] An opposite trend is found for diamines, diols, and amino alcohols; this is directly connected to the spatial extension of the H-bond network caused by the presence of two proton donor and two proton acceptor centers in these molecules.[39] Computational studies on 1-oct[22,25,26] support the view of a complex structuring of the system constituted by polar H-bond regions segregated in a hydrophobic medium. It may be expected that in long-chain alcohols the nonpolar environments are characterized by a locally larger free volume and that these regions give the largest contribution to the system compressibility. In this context, the different self-association of the two isomers may modulate the extent of interactions among the alkyl tails (i.e., interaggregate), determining differences in V_m and χ_S. For both isomers, χ_S increases almost linearly with temperature, with a greater dependence for the secondary alcohol. Thus, it appears that when the hydrogen-bonding network is more extended the increase of the χ_S with T is weaker. This is confirmed by the large temperature dependence of χ_S in neat liquid octane (see the inset of Figure 1).[37]

The viscosity (η) of the two samples is compared in Figure 2. Interestingly, η of 1-oct is smaller at lower temperatures and larger at higher temperatures. The detected behavior is not specific to the system considered. For other isomeric alcohols it is found that at low T the viscosity increases with the shielding around the polar head and that the viscosity of secondary and

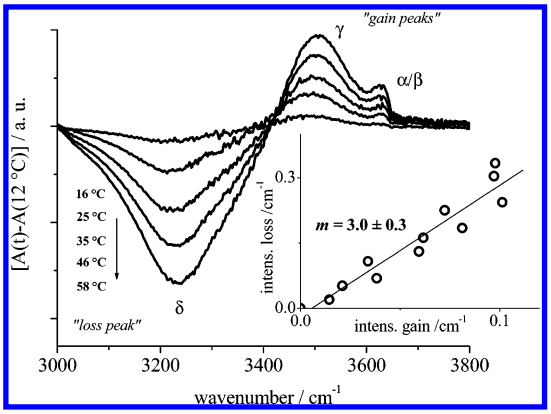

Figure 3. IR difference spectra of 2-oct in the OH stretching region calculated taking the spectrum at 12 °C as reference. Inset: correlation plot of the integrated absorbance loss vs the absorbance gain.

tertiary members decreases at a higher rate with increasing temperature.[45] The fact that 1-oct may have a lower η is somewhat counterintuitive considering V_m and χ_S trends and indicates that viscosity is not a mere function of the degree of self-association. To explain the detected behavior, it is necessary to take into account the frictional effects linked to the alkylic molecular moieties. In particular, both "hydrophobic" and H-bonding interactions drive the kinetic mechanism responsible for viscous flow, and their mutual balancing, intrinsically temperature dependent, is probably responsible for the behavior detected.

Vibrational Spectra: The OH Stretching Region. The OH stretching distributions of alcohols can be modeled considering the existence of four principal states for the OH oscillators, identified as α, β, γ, and δ.[4,21,46−50] The sharp high-frequency signal (i.e., see Figures 3 and 4) is assigned to OHs not involved as proton donors in H-bonds. This signal is attributed to both monomers (α OHs) and terminal proton acceptor OHs (β OHs). Since α and β types are not discriminated in neat liquids,[49] these oscillators are indicated as "free", non-H-donor (ND) or α/β OHs, (i.e., three-state approximation).[4,21] The broad low-frequency distribution of H-donor OHs (D) involves noncooperative OHs, resonating at around 3500 cm^{-1} (γ OHs), and oscillators participating in cooperative H-bonds at ca. 3300 cm^{-1} (δ OHs);[47,50,51] these latter dominate the neat liquid phase.[4,21] In several works the γ OHs are associated to the terminal H-donor OHs and the δ OHs to the oscillators both H-donors and H-acceptors, embedded within the hydrogen-bonded chains.[4,21,46−48] On the other hand, in a recent computational study[50] it has been shown that the γ OH (also described as dimer-like[47,50]) is the next to the last terminal non-H-donating β OH. Nevertheless, for linear aggregates the two descriptions are spectroscopically indistinguishable, and it can be assumed that for any given open chain, one "free" β OH and one noncooperative γ OH will exist, independent of the real position of this last. Quantitative differences may be significant when a large degree of branching, (i.e., OH involved in three H-bonds) is accounted for.

Rising temperature increases the fraction of γ, β, and α OHs at the expense of internal δ OHs. This situation is evidenced by the temperature-induced IR difference spectra of 2-oct, reported in Figure 3. Here the subensemble of OHs that mainly suffer the thermal changes can be detected. The difference spectra of Figure 3 closely resemble those of 1-oct.[21] The plot of the integrated intensity loss measured below the isosbestic point, as a function of the integrated intensity gain measured

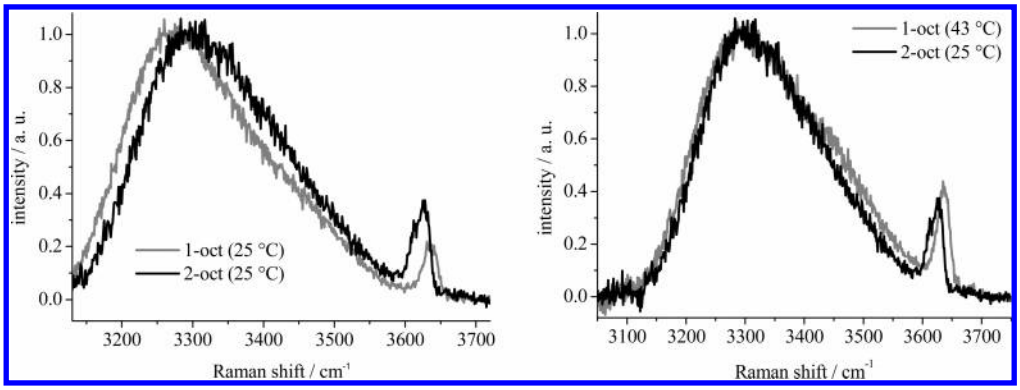

Figure 4. Comparison of isotropic Raman OH stretching spectra of 1-oct and 2-oct.

TABLE 2: Fraction of Nondonor ND Oscillators $f(\alpha/\beta)$ Obtained from Raman Data at Different Temperatures[a]

1-oct					2-oct				
T/°C	$f(\alpha/\beta)$	p_B	n_{HB}	n_a	T/°C	$f(\alpha/\beta)$	p_B	n_{HB}	n_a
					5.3	0.028	0.972	1.94	35.9
12.4	0.021	0.979	1.96	48.2					
15.5	0.023	0.977	1.96	44.0	14.9	0.043	0.957	1.91	23.4
18.3	0.026	0.974	1.95	37.9					
21.6	0.030	0.970	1.94	33.4					
25.9	0.032	0.968	1.94	30.8	25.0	0.061	0.939	1.88	16.5
29.7	0.038	0.962	1.92	26.3					
35.6	0.045	0.955	1.91	22.1	34.9	0.078	0.922	1.84	12.9
43.2	0.056	0.944	1.89	17.9	44.7	0.093	0.907	1.81	10.7
47.5	0.064	0.936	1.87	15.7					
51.6	0.071	0.929	1.86	14.1	54.5	0.116	0.884	1.77	8.62
58.5	0.074	0.926	1.85	13.5					
62.9	0.089	0.911	1.82	11.2	64.2	0.144	0.856	1.71	6.95
67.5	0.092	0.908	1.82	10.9					
72.6	0.107	0.893	1.79	9.3	74.1	0.169	0.832	1.66	5.93
77.7	0.113	0.887	1.77	8.8					
84.9	0.129	0.871	1.74	7.8					
89.7	0.135	0.865	1.73	7.4					

[a] The H-bond probability defined as $p_B = [1 - f(\alpha/\beta)]$ is also reported, together with the average number of H-bonds formed for OH (considered as both proton acceptor and donor) $n_{HB} = 2p_B$ and average aggregation number (evaluated neglecting cyclic species) $n_A = 1/(1 - p_B)$.

above the isosbestic point, shows that the spectral changes are correlated and that the conservation law for the OH population applies (inset of Figure 3). The resulting slope (m) depends on the relative absorption enhancement that a given OH type experiences in the $\delta \rightarrow \gamma$, α/β transition;[52] similar m values are found for 1-oct ($m = 3.6 \pm 0.1$[21]) and 2-oct ($m = 3.0 \pm 0.3$).

Raman Spectra. In Figure 4, the comparison of the isotropic (ISO) Raman profiles, classically defined as $I_{ISO}(\nu) = I_{VV}(\nu) - (^4/_3)I_{HV}(\nu)$, is reported for the two isomers. The frequency position of the D band at 25 °C (D = $\delta + \gamma$) is at ca. 3280 cm^{-1} for 1-oct and at ca. 3300 cm^{-1} for 2-oct (left). The OH Raman distribution of 2-oct at 25 °C compares quite well with the 1-oct OH spectrum at 43 °C (right). This suggests that liquid 1- and 2-oct mainly differ in consequence of different population percentages of similar species. The fraction of ND OHs ($f(\alpha/\beta)$) for both isomers is reported in Table 2. The values are obtained by rescaling the corresponding Raman intensity ratios in order to reproduce the ND percentages derived from NIR experiments[16] and the MD simulation of DeBolt and Kollman[22] of 1-oct at 40 °C. This comparison leads to a scaling factor of $S = 1.75$ for 1-oct, and the same value of S is also assumed to apply to 2-oct, where S measures the increase of the molar Raman cross section σ induced by the formation of H-bonds: $S = \sigma(D)/\sigma(ND)$. An enhancement of the average OH Raman activity of similar magnitude has already been proposed for water and alcohols.[52−54] Note that a unique S value leads to the correct estimation of the α/β percentages even at other temperatures (see Table 3).

TABLE 3: Percentage of Different OH "Types" Calculated Using the $f(\alpha/\beta)$ Values Obtained by Raman Data and the Sub-bands Decomposition of IR OH Profiles in Pure Liquid 1-Oct and 2-Oct (See Text for Details)[a]

1-oct				2-oct			
T/°C	% δ	% γ	% α/β	T/°C	% δ	% γ	% α/β
10.5	93.6	4.5	1.9	11.8	77.9	18.3	3.8
15.5	92.6	5.0	2.3	16.0	76.2	19.4	4.3
20.7	91.6	5.6	2.8	20.4	74.4	20.6	5.0
25.4	90.6	6.0	3.3 (4[b];2[c])	25.0	73.2	21.0	5.8
31.0	88.8	7.3	4.0	30.2	72.4	20.9	6.7
35.1	87.7	7.8	4.5	35.0	70.2	22.2	7.6
40.1	86.3 (86.2[d])	8.6 (8.6[d])	5.2 (5.2[d];5[b])	41.0	68.5	22.6	8.8
46.8	84.4	9.5	6.1	46.5	66.3	23.7	10.0
50.9	82.2	11.1	6.7	52.0	65.1	23.6	11.3
55.9	80.6	11.9	7.5	58.0	63.5	23.8	12.7
61.0	79.1	12.5	8.4				
64.4	78.1	12.9	8.9	65.0	62.0	23.5	14.4
70.3	76.8 (77.7[d])	13.2 (11.2[d])	10.0	70.0	61.0	23.3	15.7
76.0	75.2	13.8	11.0 (11.1[d])				
80.7	73.7	14.4	11.9 (12[b])				
84.2	72.7	14.7	12.6				

[a] The corresponding data obtained from NIR, MD, and MC studies are also reported. [b] Ref 16. [c] Ref 26. [d] Ref 22.

The vapor pressure of a liquid is greatly affected by the presence of H-bonding interactions. For an alcohol, the vapor pressure P_{OH} is reduced with respect to the vapor pressure of an isomeric ether P_{Et} or of a "homomorphous" alkane P_{Al} in which the O atom is replaced by a CH_2 group.[55] For primary alcohols, the relative vapor pressure reduction (i.e., P_{OH}/P_{Al}) roughly corresponds to the spectroscopic $f(\alpha/\beta)$ value evaluated by IR spectroscopy:[55]

$$P_{OH} \approx f(\alpha/\beta)P_{CH3} \quad (2)$$

Note that $f(\alpha/\beta)$ can be also regarded as the time fraction during which a molecule has lost the H-bond energy.[55] At 25 °C the vapor pressure ratios of 1-oct/nonane is $P_{OH}/P_{Al} \approx 0.02$ and that of 2-oct/2-methyl-octane is $P_{OH}/P_{Al} \approx 0.04$.[56] These values reproduce the correct order of magnitude for the $f(\alpha/\beta)$ in Table 2, indicating that the increased vapor pressure is correlated to a reduction in the degree of self-association evaluated by Raman spectra.

A Stochastic Aggregation Model. Thus, $f(\alpha/\beta)$ is the fraction of OHs not involved as donors in H-bonds, and the probability p_B that a given OH is H-bonded may be defined as[30,55]

$$p_B = 1 - f(\alpha/\beta) \quad (3)$$

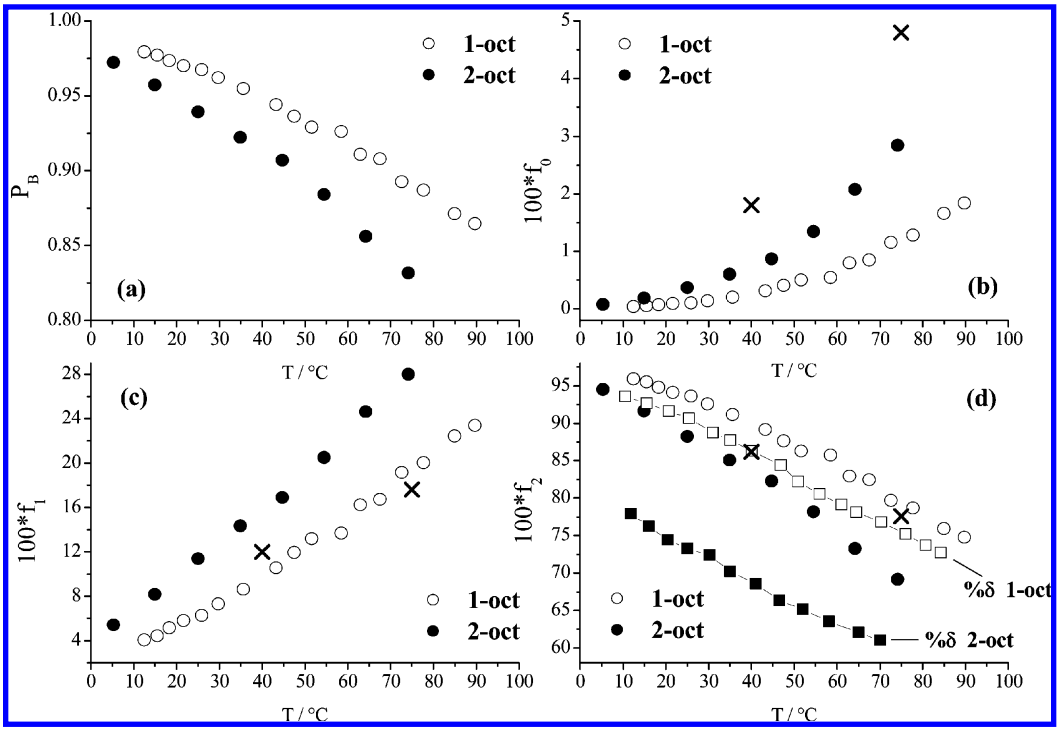

Figure 5. H-bond probability P_B (a) and percentages of OHs implicated in zero (b), one (c), or two (d) H-bonds for 1-oct and 2-oct as derived by eq 4. The MD results of DeBolt and Kollman (ref 22) (×) and the percentages of δ OHs of Table 3 are also reported (d). See text for details.

In Table 2, the p_B value obtained by Raman experiments is reported together with the average number of H-bonds contacts *per* molecule, $n_{HB} = 2\,p_B$, and the average aggregation number, $n_A = 1/(1 - p_B)$; this latter is truly indicative only if cyclic species can be neglected. The average number of HB contacts per 1-oct molecule at 25 °C is 1.94, in close correspondence with the n_{HB} of 1.96 reported in the recent Monte Carlo study of Chen and Siepmann.[26] In 2-oct the shielding increases of a factor 2 the $f(\alpha/\beta)$ fraction. As expected, p_B decreases at higher T and is in any case greater for the 1-oct isomer. The average aggregation number n_A of 1-oct is larger than that obtained in the MD simulation of DeBolt and Kollman[22] of 10.4 at 40 °C and 7.4 at 75 °C. This difference is essentially related to the presence of small cyclic aggregates in the simulation box.[22] In fact, the agreement increases at higher temperatures, when the opening of cyclic species is expected. The presence of significant contributions arising from small cyclic species is found also in the MC study of Chen and Siepmann.[26] A value of $n_A = 30$ at 25 °C is, however, well within the calculated aggregate distribution of simulation studies,[22,25,26] supporting the view of a strong self-association even at higher temperatures, when the n_A evaluation is more reliable. The value of $n_A = 30$ is also consistent with the values estimated by Huyskens and Ruelle[55] using vapor pressure for normal alcohols of different chain lengths. Their n_A values are 120, 90, 80, 65, and 55 from ethanol to hexanol. Table 2 shows that in 2-oct the average aggregation number is reduced by a factor of ca. 2/1.5 indicating important shortening of the HB species.

Liquid alcohols can be tentatively described in terms of a statistical model in which[29,30] (i) the presence of linear chain aggregates is considered, (ii) the probability that an OH is involved in a H-bond is constant (i.e., p_B does not depend on the OH position or on the aggregate length), (iii) each OH group can be implicated in the formation of zero, one, or two H-bonds (i.e., branched structures are neglected). Under these simplifying assumptions the fraction f_i of molecules with i intact H-bonds follows the binomial distribution.[29,30]

$$f_0 = (1 - p_B)^2 \qquad f_1 = 2p_B(1 - p_B) \qquad f_2 = {p_B}^2 \tag{4}$$

In Figure 5 the f_i values for both isomers are compared. The model predicts that f_0 and f_1 increase and that f_2 decreases with increasing temperature, in agreement with the experimental and MD trends. Moreover, for both isomers, the majority of the ND OHs are of β type and the fraction of α monomers (f_0) is very small, as previously found.[49] With respect to the MD results,[22] f_0 is underestimated by the stochastic model; nevertheless it leads to proper values for f_1 and f_2 (see Figure 5) giving a correct picture of the involvement of the molecules in H-bonds. An analogous agreement may be expected for the more shielded 2-isomer. Recently, a similar percolation model[29] has been successfully applied to describe IR signals of liquid water.[31]

H-Bonding Enthalpy and Entropy. The enthalpy (ΔH) and entropy (ΔS) changes associated with the free ↔ aggregates equilibrium are calculated taking the observed temperature dependence into account. The equilibrium constant is expresses in terms of donors and nondonors OHs $K = [D]/[ND]$;[25] the resulting van't Hoff plots are reported in Figure 6. The slope, $\Delta H/R$ and the intercept, $\Delta S/R$ are obtained by the linear fit of the data. The ΔH is -22.4 ± 0.5 kJ/mol and -21.9 ± 0.5 kJ/mol for 1- and 2-oct, respectively. The difference is very small, suggesting that the average strength on an H-bond is slightly dependent on the OH position. The spectroscopic ΔH values are comparable to those resulting from several calculations on alcohol aggregates[54,57−61] and reproduce the mean "thermodynamic" HB energy of the systems very well.[62] This can be evaluated by subtracting from the vaporization enthalpy ΔH_{vap} of an alcohol that of the "homomorphous" alkane, (see Table 4).

In 1-oct two energetic domains for the cooperativity enthalpy ΔH^C, obtained from the temperature dependence of the A_γ/A_δ

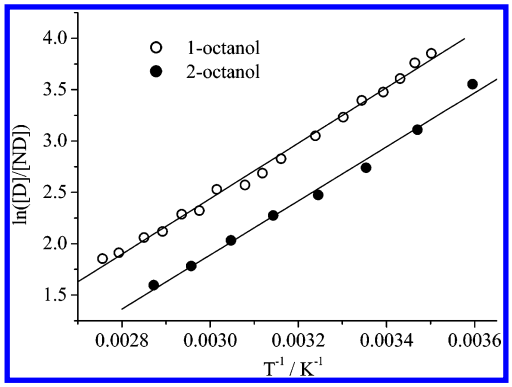

Figure 6. van't Hoff plot of the donor/nondonor concentration ratio for 1-oct and 2-oct.

TABLE 4: Comparison of the H-Bond Enthalpies (in kJ mol^{-1}) Obtained with Different Methods

	1-oct	2-oct
ΔH_H[a]	24.1	23.5
ΔH_H (Raman)[b]	22.4 ± 0.5	21.9 ± 0.5
ΔH_H (ν_{IR})[c]	22.6 ± 0.2	22.2 ± 0.2
ΔH_H (IR−HBED)[d]	27 ± 1	25 ± 1

[a] Calculated subtracting from the ΔH_{vap} of alcohols that of the "homomorphous" alkane as in ref 62; the ΔH_{vap} is calculated considering group contributions of ref 64. [b] By the van't Hoff plot of Raman data (Figure 6). [c] From the IR spectra at 25 °C using eq 5. [d] Upper limit value obtained from the IR H-bond energy dispersion (Figure 8).

absorbance ratio, were previously detected, and the occurrence of a structural transition around 40−50 °C was suggested.[21] Here, a unique regime is detected by Raman data, which provide a more averaged measure for the donor band. The average cooperative ΔH^C evaluated by IR data is −15 ± 2 kJ/mol and refers to the $\gamma \rightarrow \delta$ stabilization energy,[21] while the Raman estimate $\Delta H = -22.4 \pm 0.5$ kJ/mol is relative to the $\alpha,\beta \rightarrow \gamma,\delta$ transition. It can be assumed $\Delta H \approx f_\gamma \Delta H(\gamma) + (1 - f_\gamma)\Delta H(\delta)$ where $f_\gamma = \gamma/(\gamma + \delta)$. $\Delta H(\gamma)$ and $\Delta H(\delta)$ are the stabilization energies for γ and δ OHs, respectively. Considering $\Delta H(\delta) \approx \Delta H^C + \Delta H(\gamma)$ leads to $\Delta H(\gamma) \approx -8$ kJ/mol and a cooperativity increment $\Delta H(\delta)/\Delta H(\gamma) \approx 2.9$. A value of 2.7 is found for methanol using the Badger−Bauer rule.[51]

The calculated entropy change is −11.2 ± 0.3 and −11.9 ± 0.3 eu for 1- and 2-oct, respectively, such that the 1-oct self-association is favored for entropic reasons as well. The fact that $|\Delta S^{1-oct}| < |\Delta S^{2-oct}|$ seems in line with the presence of greater fractions of cyclic species in the more shielded isomer.[5−7,60] At 298 K, $\Delta G^{1-oct} = -2.0 \pm 0.2$ kcal/mol and $\Delta G^{2-oct} = -1.7 \pm 0.2$ kcal/mol. The consistency of our treatment is verified by comparing the 1-oct free energy at 40 °C ($\Delta G^{1-oct} = \Delta H^{1-oct} - T\Delta S^{1-oct} = -1.8 \pm 0.2$ kcal/mol) with the value calculated, as $\Delta G^{1-oct} = -RT \ln K = -1.80$ kcal/mol, in which K is derived from the MD study of DeBolt and Kollman.[22]

IR Spectra. In the previous work, IR spectra of 1-oct were modeled by means of a curve-fitting procedure.[21] Three Gaussian components, representing δ, γ, and α/β OHs, were used to reproduce spectral features. An analogous fitting procedure is applied to the 2-oct case. An example of the fitting results is reported in Figure 7. For both isomers, Gaussian functional forms with the same width and similar peak position are employed. For the 2-oct, the calculated δ band has lower relative intensity and is slightly blue-shifted. In Table 3, the population percentages calculated with the combined use of IR and Raman data are reported. The δ/γ population ratio is obtained from IR data, after correcting the extinction coefficients (ϵ) for the effect of the HB formation. The increment of the extinction coefficients caused by the formation hydrogen bonds has been previously evaluated, by studying the 1-oct/octane system at low alcohol concentration.[21] The signals due to α/β, γ, and δ species appear progressively with increasing alcohol concentration. Thus, assuming the gradual formation of monomers, open dimers, and trimers we could evaluate the concentration of α/β, γ, and δ species and then the $\epsilon(\delta)/\epsilon(\gamma)/\epsilon(\alpha/\beta)$ relative increments. The resulting population ratio δ/γ was in agreement with the MD simulation data of DeBolt and Kollman.[22] The fraction of α/β OHs is derived from the Raman data, intrinsically more sensitive to the population of "free" ND species. As can be seen from Table 3, the results are consistent with NIR,[16] MD[22], and MC[26] findings at all the temperatures. For 2-oct a considerable fraction of γ is detected; moreover, the δ/γ ratio presents quite weak temperature dependence in comparison with the case of 1-oct.[21]

The percent δ of Table 3 should roughly represent the percentage $100f_2$ resulting from the statistical model (the $100f_1$ value formally corresponds to the sum of percent β and percent γ). As can be seen in Figure 5, for 1-oct percent δ and $100f_2$ are comparable, reinforcing the suitability of both descriptions. On the contrary, the $100f_2$ value is significantly larger than the percent δ for the 2-isomer. In this case the assumption that the γ component only involves terminal OHs is probably excessively restrictive, and it may be reasonable to consider a less rigid "three-state" description, in which γ and δ OHs simply refer to weakly cooperative, and fully cooperative H-bonds, respectively.[51] Within this "relaxed" definition, the IR γ component may also include weakly cooperative OHs (i.e., f_2 OHs) completely embedded within small aggregates.

H-Bonding Enthalpy. The peak frequency of the δ component (see Figure 7), which in practice defines the maximum of the IR band, is slightly red-shifted in 1-oct with respect to that of 2-oct. The difference is 8 cm^{-1} at 15 °C and vanishes at high temperatures. The frequency difference ($\Delta\nu$) between the "free" and the H-bonded OHs, $\Delta\nu = \nu_f - \nu_{HB}$, measures the HB strength.[4,51,63] Thus the IR data suggest that the 1-isomer forms clusters with slightly stronger H-bonds; this is especially true at lower temperatures. An empirical correlation law between the H-bond enthalpy (ΔH in kJ/mol) and the frequency shift ($\Delta\nu$ in cm^{-1}) has been proposed recently as an extension of the Badger−Bauer law:[63]

$$(\Delta H)^2 = 1.92[\Delta\nu - 40] \qquad (5)$$

Taking $\nu_f = 3630$ cm^{-1} as the reference leads to ΔH values at 25 °C for the IR δ component of 22.6 and 22.2 ± 0.2 kJ/mol for 1- and 2-oct, respectively, in agreement with Raman estimations (Table 4).

The molar vaporization enthalpy ΔH_{vap} may be decomposed considering two terms:

$$\Delta H_{vap} = p_B \Delta H_{HB} + \Delta H_{NHB} \qquad (6)$$

ΔH_{HB} is the molar enthalpy of H-bond breaking, p_B is defined as in eq 3, $p_B\Delta H_{HB}$ is the molar HB contribution, and ΔH_{NHB} accounts for all of the other interactions (i.e., dipolar, van der Waals). The vaporization enthalpy ΔH_{vap} evaluated by group contributions[64] is 70.2 (1-oct) and 67.5 (2-oct) ± 0.7 kJ/mol at 25 °C, while the HB term, $p_B\Delta H_{HB}$, is 21.7 (1-oct) and 20.9 (2-oct) ± 0.2 kJ/mol. Then from eq 6 follows: ΔH_{NHB} (1-oct) = 48.5 ± 1.0 kJ/mol and ΔH_{NHB} (2-oct) = 46.6 ± 1.0 kJ/mol. In practice, the difference in the HB term of 0.8 ± 0.4 kJ/mol alone does not explain the vaporization enthalpy variation of 2.7 ± 1.4 kJ/mol; the change in nonspecific interactions must

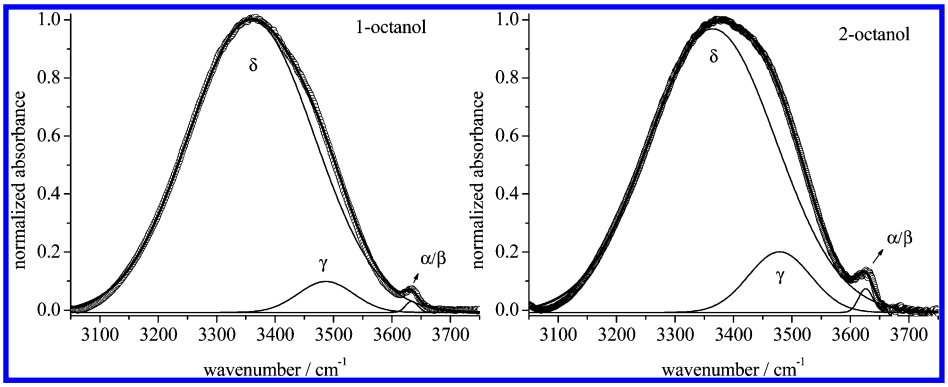

Figure 7. IR spectra of 1-oct and 2-oct at 70 °C (circles) together with the theoretical fitting (thick lines) and the fitted components (thin lines).

also be considered. The 1-oct liquid structure is described considering that the interacting polar heads are confined by a sort of "hydrophobic effect"[18,22,25,26] and that important interaggregate interactions originate from the alkylic tails.[18,25,65] The occurrence of chain interdigitation phenomena has also been invoked.[25] Thus, the data can be interpreted considering that the different topology of H-bond structures in 1- and 2-oct, also supported by other findings,[4−7] may affect the interaggregate interactions, modulating the dispersion forces among alkylic tails. In this regard, it can be inferred that linear HB aggregates, prevalent in 1-oct, lead to a more favorable packing of the alkylic chains. This picture is in line with the difference in both molar volume and compressibility discussed above. Moreover, the excess partial molar volume at infinite dilution V^E of linear alkylic solutes (i.e., hexane, ethyl ether) measured in both 1- and 2-oct is negative.[28] This indicates that linear apolar solutes can be favorably accommodated among the alkylic chains. In agreement with the previous picture, for a given solute V^E is more negative if 1-oct is the solvent.[28] Here, the liquid organization favors solute−solvent interchains packing.

Hydrogen Bond Energy Dispersion (HBED). The temperature evolution of OH profiles can be analyzed in terms of H-bonding energy dispersion $E(\nu)$ defined as[32−34]

$$E(\nu) \equiv -R[\partial \ln I(n)/\partial(1/T)] \qquad (7)$$

where R is the gas constant and $I(n)$ is the absolute Raman intensity. The same definition was recently applied to IR profiles of 1-oct in which IR absorbance $A(n)$ is considered.[4,21] IR spectra at different T have been normalized by the corresponding CH intensity to take into account density changes and variations of instrumental conditions. For both 1- and 2-oct isosbestic points (ν_{IP}) are identified; the adopted definition implies $E(\nu_{IP}) = 0$. The $E(\nu)$ distributions calculated for 1- and 2-oct are reported in Figure 8a. The small frequency difference in isosbestic points in 1- and 2-oct is irrelevant and permits a reliable comparison.

The $E(\nu)$ curves are very similar for the two alcohols, and both show a large low-frequency minimum $\nu_\delta \approx 3100-3200$ cm^{-1} assigned to δ OHs involved in H-bonds with large cooperativity. In both cases the maximum at $\nu_\alpha/\beta \approx 3640$ cm^{-1}, related to the "free" OHs, can be recognized. ν_α/β extends beyond a broad positive peak at around $\nu_\gamma \approx 3600$ cm^{-1} due to γ OHs; this latter is better defined for 1-oct. The difference is partially related to the fact that the position of the "free" OH signal in 2-oct located at lower frequency than in 1-oct (see Figures 4 and 7). This is due to the presence of different rotational isomers. As recently discussed, an oxygen lone pair may be delocalized into the antibonding orbital of a nearby CH group.[49] This occurs when the oxygen lone pair and the CH bond are in trans position and gives rise to the so-called trans

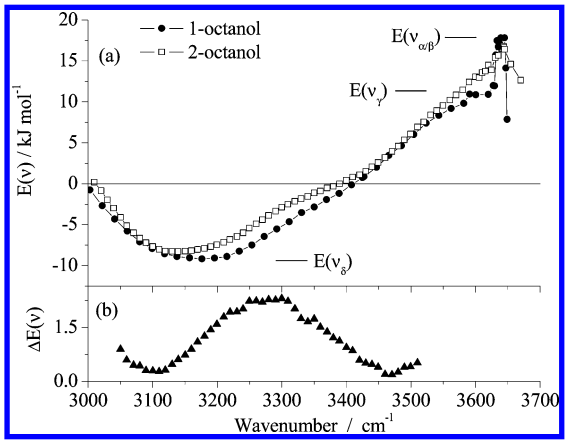

Figure 8. (a) H-bond energy dispersion $E(\nu)$ obtained from the IR OH absorbance for 1-oct and 2-oct. (b) The difference $\Delta E(\nu)$ between the 1-oct and 2-oct $E(\nu)$ curves.

intramolecular delocalization (TID). The TID induces a strengthening of the OH bond and is more active in 1-oct leading to a larger blue-shift of the "free" band.[49] The calculated $E(\nu)$ curves evidence the existence of three principal OH classes at ν values where $(\partial E(\nu)/\partial \nu)$ approaches zero; this substantiates the adopted "three-state" description.[4,21] The difference between the maximum and the minimum of the distribution is the upper limit value of the H-bond energy of the system.[33] In the present case, $E(\alpha/\beta,\delta) = E(\nu_\alpha/\beta) - E(\nu_\delta)$ corresponds to the limiting enthalpy change for the $\delta \rightarrow \alpha/\beta$ transition. $E(\alpha/\beta,\delta)$ is 27 ± 1 and 25 ± 1 kJ/mol for 1- and 2-oct, respectively. The $E(\alpha/\beta,\delta)$ values are quite similar also in view of the difficulties in defining the high-frequency ν_α/β maximum.

The minimum E_{min} of the $E(\nu)$ curve in 1-oct is at about 3180 cm^{-1} and is assigned to δ OHs of large aggregates, more efficiently stabilized by cooperative effects.[4,21] For 2-oct, the E_{min} is slightly downshifted at ca. 3150 cm^{-1}. At this frequency, the $E(\nu)$ values of the two isomers are comparable, suggesting that cooperative effects stabilize the largest clusters to a similar extent. In fact, although the H-bond energy is expected to increase with the aggregation number, the stabilization will reach a limiting value.[57,58] This convergence limit is probably attained in both 1- and 2-oct and corresponds to an HB energy of 25−30 kJ per OH mol. These values are in good correspondence with those derived by ab initio studies of methanol, ethanol, and 1-propanol clusters[57−59] and agree with MC findings on hexanol hexamers.[60] It is worth noting that the E_{min} frequency is close to the OH band position of 1-oct measured at 100 K[66] of 3253 cm^{-1} corresponding to $\Delta H = 26$ kJ/mol (eq 5).

Evident variations in the $E(\nu)$ are observed at intermediate frequencies around 3300 cm^{-1}. The difference $\Delta E(\nu)$ between 1-oct and 2-oct $E(\nu)$ curves is reported in Figure 8b. $\Delta E(\nu)$ is

symmetrically distributed around 3280 cm^{-1} and may be assigned to 1- and 2-oct aggregates that show different sensitivity to thermal variations. The frequency location indicates that the principal structural modifications involve small and/or weakly cooperative species. For these, the HB energy is expect to depend on aggregate size and geometry.[57−60] The averaged $\Delta E(\nu)$ value in the 3100−3450 cm^{-1} range is ca. 1.3 kJ/mol and accounts for a small HB energy decrease in the 2-isomer. These findings may be interpreted considering that the shielding around the polar head increases the percentages of small (and cyclic[4−7]) clusters characterized by weaker H-bonds.

Conclusions

Liquid 1-oct and 2-oct were investigated by IR, Raman, and Brillouin experiments. The less associative character of the 2-isomer is confirmed by all of the experimental data. The 1-isomer is the most interacting system, consisting of long-chain H-bond aggregates in part stabilized by favorable alkylic interactions. In 2-oct, the increased shielding around the polar head induces the formation of smaller, less cooperative species; these latter likely include cyclic aggregates.[4−7] The "OH type" description,[46−49] lately supported by the study of Stubbs and Siepmann,[50] is adequate to model the OH profiles of neat alcohols and provides evidences on the 1-oct liquid system which are in quantitative agreement with available computational studies.[22,26]

The combined use of IR and Raman data increases the correspondence between experimental and calculated OH populations,[21] giving a consistent description at all the temperatures. The system is strongly self-associated with large aggregation number n_a even at the highest temperature ($n_a \approx 7$ at 90 °C). Often tetramers are considered to dominate in liquid alcohols;[17,62] in this respect, our findings indicate that OHs implicated in clusters of four units are not prevalent in the pure sample.[22,25,26] A quantitative description is also reported for the 2-oct for which computational results are lacking. In the case of the less aggregated 2-isomer, a less rigid interpretative scheme in terms of free, weakly cooperative, and cooperative OHs seems more appropriate, in light of the increased importance of small clusters.

It is worth nothing that the discrete description of OH stretching distributions often employed in the literature[32,33,51−53,67] has been questioned especially in the case of water by several authors who argue instead for a continuum model.[68,69] In this context the partition of the broad distribution of alcohols in δ and γ OHs may appear somewhat artificial and the quantitative agreement obtained fortuitous. However, for alcohols a distinct spectral γ component can be identified in diluted conditions and in the supercritical phase as well,[21,54,70] and the presence of a distinct population of non-H-donors α/β OHs can be clearly identified (see Figures 4 and 7). Moreover, for *tert*-butyl alcohol it is possible to clearly identify even the α and β subcomponents of the "free" signal.[49] In this sense it seems that, at least for alcohols, the assumption of distinct populations of oscillators may be justified by experimental evidences.

On the basis of Raman data the H-bond probability p_B may be defined and its temperature dependence detected. This make it possible to verify theoretical predictions for pure liquid alcohols and to quantify the effect of the molecular isomerism. The temperature evolution of the HB network is reproduced considering a stochastic model,[30] which leads to predictions in reasonable agreement with IR data and MD results.[22] For 2-oct discrepancies between the statistical and "OH type" descriptions are found; this is mainly ascribed to an overestimation of γ species from the IR bands.

The average HB energy *per* OH was quantified using both Raman and IR data; the obtained values (Table 4) are in line with thermodynamic estimations.[62] In this respect, it is confirmed that the enthalpy−frequency relationship[63] (eq 5) is adequate even under high association conditions. The average H-bond ΔH value is around −22 kJ/mol and is essentially due to cooperative H-bonds dominating the liquid systems. If an average cooperative contribution $\Delta H^C \approx -15$ kJ/mol is considered,[21] than $\Delta H(\delta) \approx -23$ kJ/mol and $\Delta H(\gamma) \approx -8$ kJ/mol for the stabilization enthalpies of δ and γ OHs, respectively. The polarization effects almost triples the H-bond stability, in agreement with previous experimental findings.[51] We note that ab initio calculations on small isolated clusters lead to larger energy values for noncooperative HB and lower cooperative increments.[57−59,61] In this sense it seems reasonable that the computed HB interactions in small isolated aggregates is larger than the average values obtained in the bulk. The HB formation enthalpy obtained in the recent MC study of Stubbs and Siepmann[60] on diluted solution of hexanol is ca. −25 kJ/mol for the larger aggregate considered ($n_a = 6$) in reasonable agreement with the $\Delta H(\delta)$ value. Nevertheless, the stabilization energy of dimers is considerably larger (ca. −33 kJ/mol) than the experimental $\Delta H(\gamma)$ (dimer-like) HB of high-concentration samples.

For 2-oct the average H-bond energy is only slightly reduced, such that entropic factors are important in determining the difference in the aggregation equilibria. A higher degree of order is attributed to the HB aggregates of the 2-isomer. It is also proposed that the differing HB capability may modulate the interactions involving the alkyl molecular moieties. This is thought to be the main origin of the increased molar volume and compressibility in the 2-isomer and partially justifies the difference of vaporization enthalpies as well.

Additional information is obtained by comparing the IR H-bond energy dispersion (HBED) curves. These functions proved sensitive in detecting small energetic variation for the two samples. The HBED curves are somewhat differently distributed in the two systems, indicating the existence in 2-oct of a certain fraction of weakly cooperative species, resonating around 3300 cm^{-1}, with smaller HB energies than in 1-oct. This may be ascribed to an increased percentage of smaller, cyclic,[4−7] more ordered clusters in the 2-isomer. It confirms that the different OH location modifies the overall liquid structure changing the aggregates architecture.[4−7] Nevertheless, also in 2-oct the limiting cooperative energy value is reached. In this respect, the upper energy limit of a fully cooperative H-bond in the system is found to be 25/30 kJ/mol.

With respect to the conventional use of 1-oct in partition studies of biorelevant molecules,[14,15] in principle, the isomeric effect may represent a convenient way to control the lipophilicity of the apolar phase in order to mimic specific biological systems.[27,28]

Acknowledgment. Financial support from the Ministero dell'Istruzione, Università e Ricerca (MIUR, Roma) under the COFIN 2003 project is gratefully acknowledged.

References and Notes

(1) Jorgensen, W. L. *J. Phys. Chem.* **1986**, *90*, 1276.

(2) D'Arpano, A.; Donato, D. I.; Migliardo, P.; Aliotta, F.; Vasi, C. *Mol. Phys.* **1986**, *58*, 213.

(3) Chen, B.; Potoff, J. J.; Siepmann, J. I. *J. Phys. Chem. B* **2001**, *105*, 3093.

(4) Paolantoni, M.; Sassi, P.; Morresi, A.; Cataliotti, R. S. *J. Raman Spectrosc.* **2006**, *37*, 528.

(5) Czarnecki, M. A.; Orzechowski, K. *J. Phys. Chem. A* **2003**, *107*, 1119.
(6) Czarnecki, M. A. *J. Phys. Chem. A* **2003**, *107*, 1941.
(7) Czarnecki, M. A. *Vib. Spectrosc.* **2004**, *36*, 237.
(8) Dugue, C.; Emery, J.; Pethrick, R. A. *Mol. Phys.* **1980**, *41*, 703.
(9) Mandal, H.; Frood, D. G.; Saleh, M. A.; Morgan, B. K.; Walker, S. *Chem. Phys.* **1989**, *134*, 441.
(10) Shinomiya, T. *Bull. Chem. Soc. Jpn.* **1989**, *62*, 908.
(11) González, M. A.; Bermejo, F. J.; Enciso, E.; Cabrillo, C. *Philos. Mag.* **2004**, *84*, 1599.
(12) Talón, C.; Bermejo, F. J.; Cabrillo, C.; Cuello, G. J.; González, M. A.; Richardson, J. W., Jr.; Criado, A.; Ramos, M. A.; Vieira, S.; Cumbrera, F. L.; González, L. M. *Phys. Rev. Lett.* **2002**, *88*, 115506.
(13) Cuello, G. J.; Talón, C.; Bermejo, F. J.; Cabrillo, C. *Appl. Phys. A* **2002**, *74*, S552.
(14) Leo, A.; Hansch, C.; Elkins, D. *Chem. Rev.* **1971**, *71*, 525.
(15) Smith, R. N.; Hansch, C.; Ames, M. M. *J. Pharm. Sci.* **1975**, *64*, 599.
(16) Grunwald, E.; Pan, K.; Effio, A. *J. Phys. Chem.* **1976**, *80*, 2937.
(17) Iwahashi, M.; Hayashi, Y.; Hachiya, N.; Matsuzawa, H.; Kobayashi, H. *J. Chem. Soc., Faraday Trans.* **1993**, *89*, 707.
(18) Franks, N. P.; Abraham, M. H.; Lieb, W. R. *J. Pharm. Sci.* **1993**, *82*, 466.
(19) Vahvaselkä, C. S. V.; Serimaa, R.; Torkelli, M. *J. Appl. Crystallogr.* **1995**, *28*, 189.
(20) Marcus, Y. *J. Solution Chem.* **1990**, *19*, 507.
(21) Paolantoni, M.; Sassi, P.; Morresi, A.; Cataliotti, R. S. *Chem. Phys.* **2005**, *310*, 169.
(22) DeBolt, S. E.; Kollman, P. A. *J. Am. Chem. Soc.* **1995**, *117*, 5316.
(23) Best, S. A.; Merz, K. M., Jr.; Reynolds, C. H. *J. Phys. Chem. B* **1999**, *103*, 714.
(24) De Oliveira, C. A. F.; Guimarães, C. R. W.; De Alencastro, R. B. *Int. J. Quantum Chem.* **2000**, *80*, 999.
(25) McCallum, J. L.; Tieleman, D. P. *J. Am. Chem. Soc.* **2002**, *124*, 15085.
(26) Chen, B.; Siepmann, J. I. *J. Phys. Chem. B* **2006**, *110*, 3555.
(27) Bernazzani, L.; Bertolucci, M.; Conti, G.; Mollica, V.; Tiné, M. R. *Thermochim. Acta* **2001**, *366*, 97.
(28) Bernazzani, L.; Mollica, V.; Tiné, M. R. *Fluid Phase Equilib.* **2002**, *203*, 15.
(29) Stanley, H. E.; Teixeira, J. *J. Chem. Phys.* **1980**, *73*, 3404.
(30) Bertolini, D.; Cassettari, M.; Ferrario, M.; Grigolini, P.; Salvetti, G. *Memory Function Approaches to Stochastic Problems in Condensed Matter*; Evans, M. W., Grigolini, P., Pastori Parravicini, G., Eds.; Advances in Chemical Physics Series, Vol LXII, 277; J. Wiley: New York, 1985.
(31) Brubach, J.-B.; Mermet, A.; Filabozzi, A.; Gerschel, A.; Roy, P. *J. Chem. Phys.* **2005**, *122*, 184509−1.
(32) Hare, D. E.; Sorensen, C. M. *J. Chem. Phys.* **1990**, *93*, 6954.
(33) Walrafen, G. E. *J. Chem. Phys.* **2004**, *120*, 4868.
(34) Beta, I. A.; Sorensen, C. M. *J. Phys. Chem. A* **2005**, *109*, 7850.
(35) Musso, M.; Torii, H.; Ottaviani, P.; Asenbaum, A.; Giorgini, M. G. *J. Phys. Chem. A* **2002**, *106*, 10152.
(36) Uemura, T.; Saito, S.; Mizutani, Y.; Tominaga, K. *Mol. Phys.* **2005**, *103*, 37.
(37) Sassi, P.; Marcelli, A.; Paolantoni, M.; Morresi, A.; Cataliotti, R. S. *J. Phys. Chem. A* **2003**, *107*, 6243.
(38) Aliotta, F.; Ponterio, R.; Salvato, G.; Musso, M. *J. Phys. Chem. B* **2004**, *108*, 732.
(39) Rodnikova, M. N.; Val'koskaya, T. M.; Kartzev, V. N.; Kayumova, D. B. *J. Mol. Liq.* **2003**, *106*, 219.
(40) Sassi, P.; Morresi, A.; Paliani, G.; Cataliotti, R. S. *J. Raman Spectosc.* **1999**, *30*, 501.
(41) Buford, D. S.; Srivastava, R. *Thermodynamic Data for Pure Compounds Part B*; Elsevier, 1986.
(42) Lepori, L.; Gianni, P. *J. Solution Chem.* **2000**, *29*, 405.
(43) Marcus, Y.; Hefter, G. T. *J. Mol. Liq.* **1997**, *73*−*74*, 61.
(44) Povey, M. J. W.; Hindle, S. A.; Kennedy, J. D.; Stec, Z.; Taylor, R. G. *Phys. Chem. Chem. Phys.* **2003**, *5*, 73.
(45) Zéberg-Mikkelsen, C. K.; Quiñones-Cisneros, S. E.; Stenby, E. H. *Fluid Phase Equilib.* **2002**, *194*−*197*, 1191.
(46) Woutersen, S.; Emmerichs, U.; Bakker, H. J. *J. Chem. Phys.* **1997**, *107*, 1483.
(47) Gupta, R. B.; Brinkley, R. L. *AIChE J.* **1998**, *44*, 207.
(48) Gaffney, K. J.; Davis, P. H.; Piletic, I. R.; Levinger, N. E.; Fayer, M. D. *J. Phys. Chem. A* **2002**, *106*, 12012.
(49) Palombo, F.; Paolantoni, M.; Sassi, P.; Morresi, A.; Cataliotti, R. S. *J. Mol. Liq.* **2006**, *125*, 139.
(50) Stubbs, J. M.; Siepmann, J. I. *J. Am. Chem. Soc.* **2005**, *127*, 4722.
(51) Luck, W. A. P. *J. Mol. Struct.* **1998**, *448*, 131.
(52) Walrafen, G. E.; Fisher, M. R.; Hokmabadi, M. S.; Yang, W.-H. *J. Chem. Phys.* **1986**, *85*, 6970.
(53) Hare, D. E.; Sorensen, C. M. *J. Chem. Phys.* **1990**, *93*, 25.
(54) Lalanne, P.; Andanson, J. M.; Soetens, J.-C.; Tassaing, T.; Danten, Y.; Besnard, M. *J. Phys. Chem.* A **2004**, *108*, 3902.
(55) Huyskens, P.; Ruelle P. *J. Mol. Liq.* **2000**, *88*, 87.
(56) P_{vap} of 1- and 2-oct are from ref 41, P_{vap} of nonane is from the NIST Chemistry webbook:www.webbook.nist.gov, and P_{vap} of 2-methyl-octane is derived by the Riedel equation as described in www.pirika.com.
(57) Hagemeister, F. C.; Gruenloh, C. J.; Zwier, T. S. *J. Phys. Chem. A* **1998**, *102*, 82.
(58) Ludwig, R.; Huelsekopf, J. *J. Mol. Liq.* **2000**, *85*, 105.
(59) Sum, A.; Sandler, S. I. *J. Phys. Chem. A* **2000**, *104*, 1121.
(60) Stubbs, J. M.; Siepmann, J. I. *J. Phys. Chem. B* **2002**, *106*, 3968.
(61) Fileti, E. E.; Chaudhuri, P.; Canuto, S. *Chem. Phys. Lett.* **2004**, *400*, 494.
(62) Benson, S. W. *J. Am. Chem. Soc.* **1996**, *118*, 10645.
(63) Iogansen, A. V. *Spectrochim. Acta, Part A* **1999**, *55*, 1585.
(64) Bosaøová, P.; Svoboda, V. *Fluid Phase Equilib.* **1995**, *105*, 27.
(65) Sassi, P.; Paolantoni, M.; Cataliotti, R. S.; Palombo, F.; Morresi, A. *J. Phys. Chem. B* **2004**, *108*, 19557.
(66) Lutz, B.; Scherrenberg, R.; van der Mass, J. *J. Mol. Struct.* **1988**, *175*, 233.
(67) Corcelli, S. A.; Skinner, J. L. *J. Phys. Chem. A* **2005**, *109*, 6154.
(68) Efimov, Yu. Ya.; Naberukhin, Yu. I. *Mol. Phys.* **2003**, *101*, 459.
(69) Smith, J. D.; Cappa, C. D.; Wilson, K. R., Cohen, R. C.; Geissler, P. L.; Saykally, R. J. *Proc. Natl. Acad. Sci. U.S.A.* **2005**, *102*, 1417.
(70) Lalanne, P.; Tassaing, T.; Danten, Y.; Besnard, M. *J. Mol. Liq.* **2002**, *98*−*99*, 201.